High pressure: one of the many tools to study material properties at extreme conditions

Nandini Garg*

High Pressure and Synchrotron Radiation Physics Division, Bhabha Atomic Research Centre, Mumbai 400 094, India

High pressure is a powerful and clean variable, which when applied can bring about large changes in structure and properties of materials. It can be used to simulate the conditions found deep inside the earth or in different planetary interiors. It is widely used in chemical industry, especially when the chemical reaction products have lower volumes than the initial reactants, and also in the food preservation industry, where it ensures that aromas and flavours are not lost even after preservation. Materials under pressure can be studied both theoretically and experimentally. In this article apart from discussing how to set up a basic high pressure experiment using the DAC, some examples have been elaborated to show how both experiments and theory complement each other and both put together can help in a deeper understanding of the changes brought about by application of high pressure.

Keywords: Germanium dioxide, high pressure, material properties.

Introduction

SINCE a major part of the universe is subjected to extreme pressure, temperature or electric and magnetic fields, scientists have put in a lot of effort to understand the effect of these extreme conditions on matter and its properties. If we apply pressure in excess of a million atmospheres we can understand the structure and properties of materials deep in the earth or cores of stars and planets. On the other hand study of matter at temperatures ~2 trillion degrees would help in understanding very different states of matter and may be the evolution of the universe. Simultaneous application of extreme pressure and temperature, can help in realizing nuclear fusion in the laboratory thus unravelling several secrets in astrophysics[1]. It is well known that several materials show exotic properties like superfluidity, superconductivity, etc. at very low temperatures. Even under extreme magnetic fields >10^5 Tesla, a new kind of chemical bond (perpendicular paramagnetic bond) may exist, which may enable bonding of H_2 in the triplet state[2].

Study of materials at high pressure is fascinating as, when compared to all other physical variables, it spans almost ~50 orders of magnitude, i.e. 10^{-24} GPa in intergalactic space to 10^{26} GPa at the centre of neutron stars[3]. Research on the effect of dynamic pressure on say, steel and concrete, could help us to design a promenade or a building which could withstand the dynamic pressures experienced by the crashing of waves or a bomb blast. Similarly understanding the effects of static pressure on different minerals deep inside the earth could enable us to synthesize some of the exotic minerals spewed out by mother earth. The deep sea expedition by the famous film director James Cameron has shown the existence of life even at the bottom of the Mariana trench where the static pressure is ~1 Kbar (ref. 4). A deeper understanding of the effect of pressure on these organisms could help us to understand the beginning of life on earth[5,6].

Subjecting matter to high pressure or low temperature, essentially results in a reduction of the inter-atomic distances. However, there is a fundamental difference between both these processes. Application of pressure leads to an increased overlap of the outermost orbitals of the constituent atoms and thus increases the repulsive forces. This alters or deforms the inter-atomic potential. However lowering of temperature essentially reduces the vibrational energy of atoms. In this case also the mean distance between atoms reduces, but, the reduction is due to anharmonicity of inter-atomic potentials in real solids. Application of pressure has more pronounced effects than lowering of temperature as the change in Gibbs-free energy per GPa is 150 times the change brought about per degree centrigrate[7]. So in the former case when the repulsive forces become large due to increased overlap of outermost orbitals, the atoms in the system try to lower the free energy by rearranging themselves. This may lead to different kinds of phase transitions and the new phases could be manifested with different interesting properties[8]. Even on lowering of temperature we can encounter phase transitions involving structural changes or simply changes in properties of the system, but, the effects are far less pronounced than observed at high pressure.

In the past, knowledge of how diamonds were made deep inside the earth helped scientists make high pressure high temperature (HPHT) diamonds in the laboratory, which is now a big industry all over the world[9]. Cubic boron nitride (a very hard material) synthesized at HPHT

*e-mail: nandini@barc.gov.in

by Wentorf et al.[10] is widely used as an abrasive, in making tools for machining, grinding, drilling and cutting. It is a much better alternative for diamond in the steel industry or say in the oil and gas industry. In recent times strongest known materials are nano polycrystalline diamonds[11,12] or nano crystalline diamonds[13] synthesized at HPHT. Their extraordinary properties like extreme hardness, thermal stability, fracture toughness, and wear resistance have led to their commercial production for usage in manufacturing of hard tools, etc.[14,15].

Study of materials at high pressure, also helps to quell our basic curiosity about structure of the earth or distant planets and stars in the universe, as can be seen by some recent interesting studies. For example last year, McWilliams et al.[16] carried out infrared absorption experiments on noble gases and tried to provide an understanding about the slow rate of cooling of the outer atmosphere of white dwarf stars, contrary to earlier predictions[17,18]. These authors showed that as observed in amorphous silicon[19], even in noble gases like He, optical absorption was dominated by localized defect states within the band gap and was not due to free electrons. Since optical opacity caused by free electrons is less than that of the localized defect states it is understandable why the earlier predictions were showing a higher rate of cooling[16]. In another study, formation of seifertite a polymorph of SiO_2 at 11 GPa, solved the long lasting Seifertite puzzle. (The presence of this polymorph in achondritic shocked meteorites formed on Mars and moon could not be explained and had been coined the Seifertite puzzle.)[20] Recent shock melting studies on stishovite revealed that high pressure liquid SiO_2 is electrically conducting and could contribute to large magnetic fields in very large terrestrial exoplanets. These magnetic fields are similar to those contributed by iron cores of smaller planets like our earth[21].

With the help of variable composition evolutionary algorithms combined with *ab initio* calculations, several new binary and ternary stoichiometric compounds of the Mg–Si–O system like SiO_3, SiO, $MgSiO_3$, $MgSi_3O_{12}$ have been predicted to form at ~TPa pressures. This information can be used to model and understand the interiors of giant exoplanets[22]. Wang et al.[23] have shown that contrary to earlier understanding, carbonic acid could be a stable species in the aqueous fluids found in the subduction zone of the earth ($P > 2.4$ GPa). Even simple oxides of iron like hematite and magnetite decompose at 60–70 GPa and 2500 K to release large amounts of oxygen and form novel oxides of iron. These experiments suggest the presence of an oxygen-rich liquid in the deep interiors of the earth[24]. Thus it can be seen that these new studies on carbonic acid and iron oxides can be used in better geochemical modelling of the earth.

It was predicted several decades ago that hydrogen gas when subjected to pressure would metalize and become superconducting at room temperature[25–27]. Several research groups around the world are trying hard to metallize hydrogen, as it could be the key to open up the secrets of our solar system and also due to its potential technological applications in electronics[28]. However, even though several high pressure phases of hydrogen have been discovered, no research group has been able to unambiguously prove the existence of metallic hydrogen till date[29–32]. Recently Drozdov et al.[33] could show that when H_2S was subjected to ~90 GPa pressure it became superconducting at 203 K, the highest reported T_c so far. They have shown that H_2S actually dissociates to H_3S at high pressure which is responsible for the superconducting transition. *Ab initio* studies by Ge et al.[34], predict that T_c can be further raised to 280 K by partially substituting sulphur in H_2S with phosphorous. Application of pressure can alter chemistry, by formation of non-stoichimetric compounds, as observed in common rocksalt or could make non reacting noble gases reactive[16,35]. Recently high pressure chemical reactions leading to formation of unexpected new stable stoichiometric calcium carbides were predicted by theory and vetted by experiments[36]. However, it is not necessary that only very high pressures can bring about significant useful changes, which can be used by industry. Exploiting the negative claperyon slope (i.e. melting temperature decreases at high pressure) of water, sub-zero temperatures can be used for storage of blood cells, stem cells, human organs, etc. without the need to freeze them[37]. A good example of high pressure induced chemical reactions is polymerization of the biocompatible polymer 2-(hydroxyethyl) methacrylate (HEMA) on pressure release from 6 GPa. Polymerized HEMA can have a lot of medical applications when formed in the absence of toxic initiators[38]. A widely used technique for hydrogen production is the treatment of vapourized hydrocarbons with steam at high pressure (15–40 bar) high temperature (650–950°C) in the presence of photocatalysts[39].

In the food preservation industry also, high pressure, or high pressure combined with TiO_2-UV photocatalysis is widely used to inactivate bacterial pathogens[40,41]. The covalent bonds in food items are responsible for their flavour, colour, texture and nutritive content[37]. These bonds do not get affected at the normal pressures of 300–600 MPa to which these food items are subjected. Thus the food items retain their sensory properties but are free from pathogens, microorganisms and food spoiling enzymes, which lead to their decay. For example strawberry jam when processed at 294 MPa for 20 min retains 95% of vitamin C and its flavour and gets rid of the yeast and bacteria which are responsible for its spoilage[42,43].

Based on the Le Chatliers principle if a systems equilibrium is disturbed by application of temperature pressure, etc., the reaction proceeds in a direction which reduces the effect of the change. So if in a reaction the products of the reaction have lower molar volume, application of pressure will enhance the rate of reaction. For

example is the famous Haber process for synthesis of ammonia pressure enhances the rate of production of ammonia. It is also interesting to note that calcium carbonate deposits are not found on the floor of the Pacific ocean but are found in the Atlantic ocean. This is because the dissolution of calcium carbonate proceeds with a reduction in volume and the pressure at the bottom of the Pacific ocean helps to dissolve calcium carbonate from the skeletons of fishes, etc.[44].

Thus we see that application of pressure is an extremely powerful and clean variable which brings about large changes in structure and properties without changing the chemical composition or thermal energy of the system. It helps us to understand the relationship between structure and properties and also helps us to design new materials for different applications.

Methods and diagnostics

Several experimental[45,46] and theoretical methods have been devised/formulated to understand the pressure response of different materials, which depend on peak pressures as well as strain rates. The dynamics of the pressure response can vary from 10^{-17} s^{-1} to 10^7 s^{-1} as observed in slow movement of tectonic plates or subjecting materials to shock pressures. In many experiments when it is difficult to attain the exact temperature and/or pressure conditions or when we want to understand the changes in different materials at the atomistic levels we can take the help of theoretical methods. There are several theoretical methods like classical molecular dynamics (CMD)[47], *ab initio* molecular dynamics (AIMD)[48], Monte Carlo calculations[49], etc. which can be used. We can also predict and design new crystal structures with the help of the new evolutionary algorithms like the USPEX, etc.[50].

In the laboratory high dynamic pressures (generating strain rates between 10^4–10^{11} s^{-1}) can be generated with the help of gas guns (~7 Mbar), explosives or with the help of pulsed high power lasers (~TPa). Static pressures (generating strain rates between 10^{-4}–10^{-2} s^{-1}) can be obtained with the help of diamond anvil cells or large volume presses. Though most of the diamond cells (DAC) can easily attain pressures of 50 GPa, recent developments by Natalia *et al.*[51] have raised the limit of static pressures obtainable in the laboratory to the TPa regime. In the large volume presses also using tungsten carbide anvils we can reach 30 GPa easily[52], but usage of sintered diamond anvils raises the pressure limit to 100 GPa (ref. 53). Apart from a few studies using the dynamic DAC the strain rate region of 10^{-2}–10^4 s^{-1} is largely unexplored[54].

In this article the main focus is on the static high pressure technique using the diamond anvil cells. The DAC is a simple device comprising two gem quality diamonds cut at the tip to create a flat surface (culet) of $\phi \sim 300$–400 µm (Figure 1).

These diamonds are mounted on two different flat backing plates of the piston and cylinder as shown in Figure 2 *a* and *b*. The piston diamond can be pressed against the cylinder diamond with the help of screws or lever arms which work on the nut cracker principle (Figure 2 *c*). Typically a thin metal (steel, inconel, tungsten, rhenium, copper beryllium, boron, beryllium) gasket of ~120 to 250 µm, is compressed between the diamonds to the required thickness (30–120 µm) (Figure 1 *a* and *b*). Subsequently a small hole is made at the centre of the diamond indentation and this thin sheet is then remounted on the diamond anvil (Figure 1 *c*). This hole acts as a sample chamber and is filled with ~100 µg of sample, along with the pressure marker and a fluid/gas medium for applying hydrostatic pressure around the sample material. The sample chamber is sealed by pushing the piston into the cylinder and the DAC is ready to carry out different kinds of experiments.

Several diamond anvil cells (Figures 2 and 3) have been developed by us to carry out high pressure, powder and single crystal diffraction studies and infrared absorption (IR) studies. Some of these cells are capable of achieving pressures of ~1 Mb. Beryllium backing plates fabricated in house, were used for the DAC used for single crystal studies. Usage of these backing plates helped to collect the full diffraction rings of polycrystalline samples at high pressure compared to the partial rings collected with the slotted geometry of the earlier tungsten backing plates. It also helped to increase the Q range of measurement (Figure 4).

High pressure DAC based IR absorption studies were initiated for the first time in the country at the IR absorption beamline at INDUS 1 (ref. 55). With the help of hyperion microscope the IR beam from the Globar source could be easily focused onto the sample in the diamond anvil cell and the data was collected with the help of the FTS spectrometer. Since the working distance of the 15× lens of the microscope places a constraint on the size of DAC, the ETH DAC design was modified and the cell was fabricated at the BARC central workshop, specially for high pressure infrared absorption studies. Also, since natural diamonds have large absorption bands as shown in Figure 5 *a*, it becomes difficult to study the IR spectra inside the diamond anvil cell, specially in the 1000–1500 cm^{-1} region. To overcome this problem synthetic (CVD) diamonds (grown by D. S. Mishra of IIT Mumbai, India) were used for the IR DAC as they have fewer absorption bands as shown in Figure 5 *b*. However, even these diamonds are not suitable to collect the IR absorption spectra in the 2000 cm^{-1} region and to specifically measure the spectra in this band, (like the absorption band of CN stretch in $Ag_3Co(CN)_6$) moissanite anvils were used. These anvils do not have a very strong absorption band in this region as shown in Figure 5 *c*.

To get a good IR spectra or good X-ray diffraction pattern from the powder samples, sample preparation has to
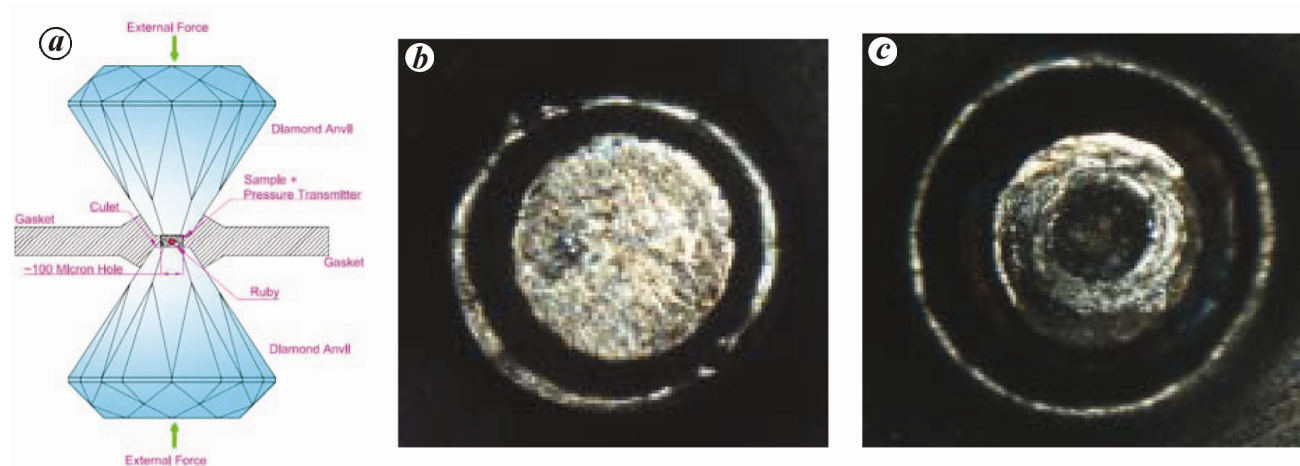
Figure 1. *a*, A schematic depicting the diamond anvils in opposing geometry with the gasket, sample and ruby. Mostly diamonds are used as anvil material for high pressure studies because of their hardness and excellent transparency to electromagnetic radiation extending from the far infrared to X-ray and γ-ray energies. However, anvils like sapphire, ruby and moissanite have also been used depending upon the requirement of the experiment[128–130]. *b*, An indented gasket showing the diamond indentation. *c*, Gasket with a 100 µm central hole which acts as the sample chamber.
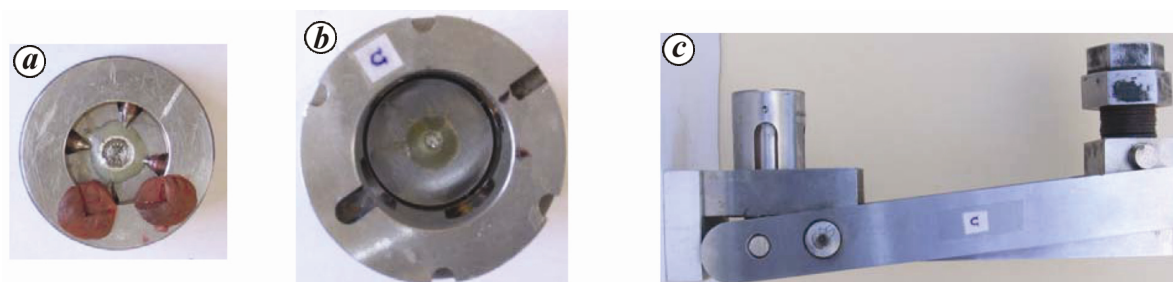

Figure 2. *a*, *b*, Diamond anvil, mounted on the piston and cylinder of the Mao Bell kind of DAC. *c*, The lever arm which helps in applying pressure to the samples in the diamond anvil cell.

be done careful. In the case of powder X-ray diffraction the samples should be finely powdered to avoid a spotty diffraction pattern due to micro-crystallites as shown in Figure 6 *a*. However, samples sensitive to non-hydrostatic stresses, tend to transform to new phases when ground in a pestle mortar and hence care must be taken while preparing the powders.

For a good IR absorption spectra the sample has to be diluted by mixing it with either CsI or KBr such that the observed absorption peaks do not saturate. In these studies the KBr and CsI matrix also acts as a pressure transmitting medium (PTM). However, for X-ray diffraction and Raman spectroscopic studies, solid pressure transmitters are generally not used. While choosing a PTM it has to be ensured that it does not have diffraction peaks or Raman vibrational modes, which interfere with the experiment. In most of the experiments, a mixture of organic liquids, like methanol ethanol (4 : 1) is used. This remains quasihydrostatic till ~10 GPa (ref. 56). But, if an inert or quasihydrostatic environment is desired in the sample chamber up to higher pressures, gases can also be used as PTM. Unlike liquid and solid pressure transmitters, these gases need either cryogenic loading or com-

pressed gas loading. Cryogenic gas loading can be carried out making a special chamber, mounted with a two-step locking device[57]. However, based on the same principle we developed a very simple cryogenic gas loading system with which Argon gas (quasi hydrostatic limit ~18 GPa)[56] can be easily loaded into the sample chamber (Figure 7). A tin can (any waste empty can) is wound by a hollow copper tube which is connected to a high purity Argon (99.99%) cylinder as shown in Figure 7. The Mao Bell cell can be put inside the tin cylinder (A) and this cylinder can now be put inside a bigger thermocol box (B). Argon gas is passed through the tubing to remove any traces of moisture etc. Subsequently liquid nitrogen filled into the outer thermocol box (immersing the copper tubing), results in liquification of Argon. Once the DAC is half submerged in liquid Argon up to the level of the sample, it is clamped. The main disadvantage of this type of loading is that the initial pressures cannot be finely controlled and many a time the initial pressure is a few GPa. Also ensuring that the sample does not get dislodged because of the bubbling of liquid argon is a bit tricky.

Determining the exact pressure that the sample is experiencing is an important part of high pressure
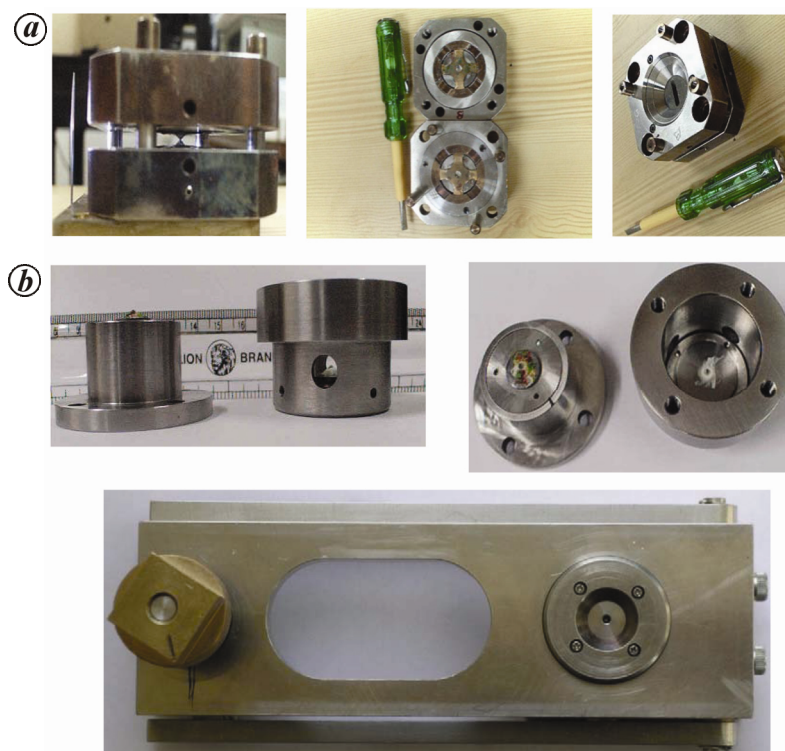
Figure 3. *a*, DAC developed for single crystal diffraction and IR studies. *b*, Short Mao Bell kind of cell equipped with beryllium backing plate or cubic boron nitride backing plate and capable of attaining ~1 Mbar pressure.
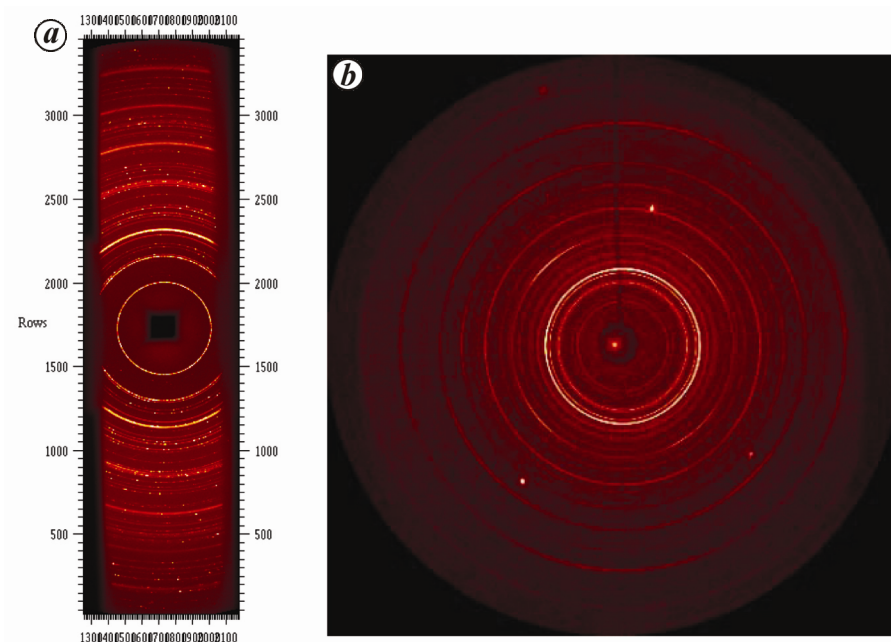

Figure 4. *a*, Powder diffraction pattern with the slotted slit geometry. *b*, Full powder diffraction rings collected with the beryllium backing plate.

experiments. Mostly we use secondary pressure standards which have been identified by calibrating some pressure dependent variable (fluorescence, vibrational mode, phase transition pressures, etc.) with the primary pressure scale. The choice of pressure standard is based on the requirements of an experiment. For example the pressures
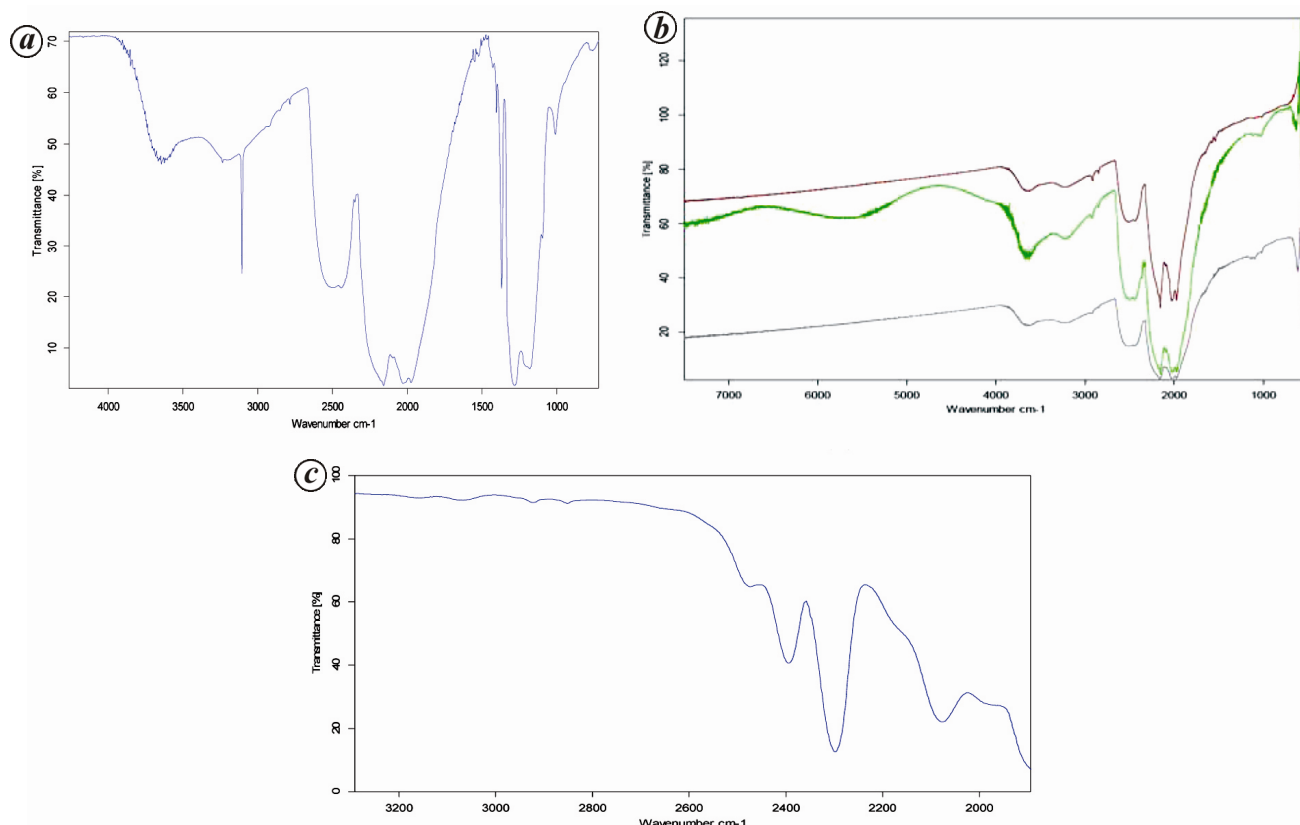
Figure 5. IR absorption spectra of (*a*) natural diamond, (*b*) synthetic (CVD) diamond and (*c*) moisannite.
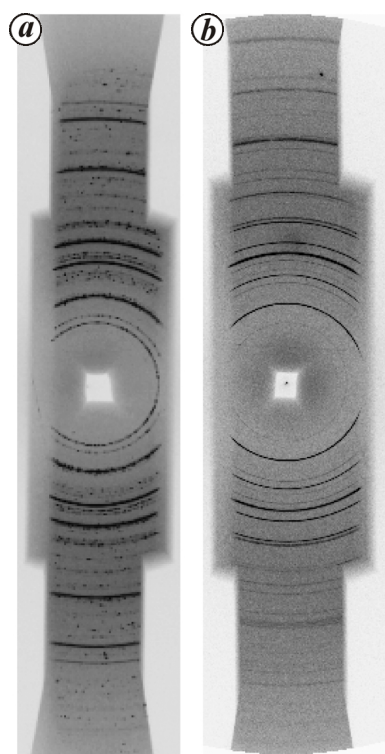

Figure 6. The two-dimensional powder diffraction pattern *a*, The spotty nature of the diffraction shows that the sample is poorly ground. *b*, The smooth diffraction lines obtained from a good powder.
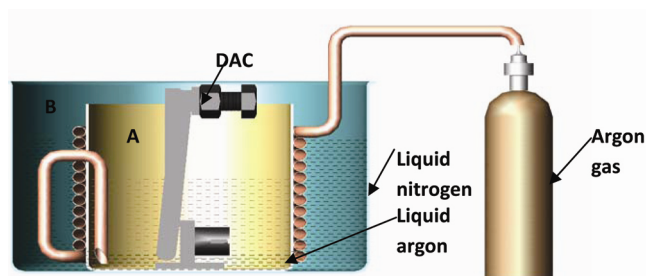

Figure 7. Cryogenic gas loading system developed in our lab. It shows the inner tin A and the outer thermocol box B. The DAC is inside the inner tin A.

in large volume presses are calibrated by interpolating between the phase transition pressures of materials like bismuth which show large changes in resistance at some fixed pressures. However, since the diamond anvil cell has an optical window, the 'ruby fluorescence scale' is mostly used to measure the pressure, which would be difficult in the case of a large volume press[58–62]. For X-ray diffraction experiments the pressure can be measured *in situ*, by using the previously determined equation of state of metals like Au, Pt, Ag, NaCl, etc.[63]. However, it should be ensured that the sample and the internal standards do not have overlapping diffraction peaks. Also, the internal standard should not undergo a phase transformation in the pressure range of the desired experiment.

Once the sample chamber is loaded with the sample, pressure marker and the pressure transmitting medium, the DAC is sealed and is ready to carry out different experiments like X-ray diffraction (single crystal and powder), Raman and Brillouin spectroscopic studies, IR absorption and reflection studies, transport property measurements, magnetic susceptibility studies, etc. All these experimental facilities exist in HP&SRPD at Trombay. However, to carry out high pressure X-ray diffraction experiments in the diamond anvil cell, an extreme condition beamline was also developed at INDUS2 Indore[64]. At this beamline the beam can be focused down to less than 100μ and can thus avoid contaminating the diffraction pattern from the gasket peaks. Also the tiny sample in the diamond anvil cell can be aligned into the beam with ease by using the software developed at HP&SRPD. This beamline (Figure 8) has a provision to carry out experiments in both angle dispersive and energy dispersive geometry.

Some research problems

From the introduction it is apparent that most of the recent high pressure studies have both an experimental proof and a theoretical backing explaining the different results. At HP&SRPD, Trombay, several theoreticians and experimentalists work hand in hand to understand the

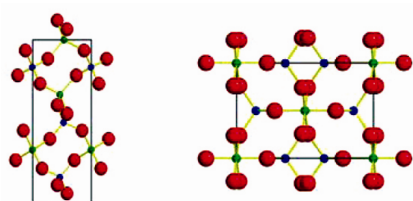**Figure 8.** Picture showing the ECXRD BL11 beamline at INDUS2 in the energy dispersive mode.

Figure 9. Quartz and Cmcm phase of $AlPO_4$.

high pressure behavior of different kinds of materials like geophysically relevant materials, nuclear encapsulants, organic, organic-inorganic, magnetic, nanomaterials, etc. In this article a few of these studies have been discussed which highlight the importance of having both experimental and theoretical understanding of the high pressure behaviour of these materials.

Berlinite (AlPO$_4$)

There have been several high pressure studies on berlinite, as it is iso-structural to quartz and hence is geophysically relevant. More than two decades back berlinite created a lot of flutter in the scientific community as laboratory X-ray diffraction experiments showed that it became amorphous at high pressure but reverted back to the original single crystal retaining the same orientations on pressure release[65]. This understanding resulted in it being termed as memory glass. Our laboratory experiments on powdered berlinite also yielded the same results[66,67]. There were several theoretical explanations for this unusual behaviour of berlinite in which the most striking and pictographic explanation was by Tse and Klug[68], wherein they showed that the spiralling AlO_4 and PO_4 tetrahedra distort, and smoothly rotate into empty spaces in the crystal on application of pressure and just unwind on release. However, subsequent enthalpy calculations indicated that the cmcm phase of $AlPO_4$ was stable beyond 12 GPa and the amorphization in the parent quartz phase could have been a result of kinetic frustration[69]. Even Gillet et al.[70] showed that the high pressure phase of berlinite was not amorphous, and iso-structural α-FePO$_4$ and α-GaPO$_4$ were shown to transform from alpha to cmcm phase[70–72]. To reconcile with these results we carried out molecular dynamical calculations starting with a larger number of atoms ($6 \times 6 \times 4$ unit cells with 2592 atoms, to avoid the observation of disorder caused by the limited number of atoms) in our macro cell. Our studies showed that berlinite was not X-ray amorphous even at 30 GPa. The cmcm phase could neither be stabilized at ambient pressure, nor could be observed in a direct transformation from berlinite to the cmcm phase. However, it could be stabilized on suddenly pressurizing the system to beyond 20 GPa (similar to dispersing a cmcm phase in an elastomer and observing the shock response) indicating that it indeed had a range of stability at high pressure[73]. Our subsequent X-ray diffraction experiments at an intense X-ray source (Spring 8) showed that the berlinite phase could be observed till 40 GPa coexisting with a poorly crystallized cmcm phase beyond 11 GPa (ref. 74). The poor crystallanity of the cmcm phase could be the reason why earlier X-ray diffraction studies concluded amorphization of berlinite. In fact years later, Pellicer Porres et al.[75] could overcome the large kinetic resistance in the formation of the cmcm

phase by laser annealing the sample at 14 GPa, resulting in a fully crystallized cmcm phase. These studies indicate that if we have a weak X-ray probe or if the high pressure phase is poorly crystalline we should be cautious while concluding amorphization. Also while carrying out classical MD calculations we should ensure that the number of atoms is large enough such that at least the central atoms of the chosen macro cell are able to depict the pressure response closely.

Germanium dioxide

GeO_2 in its various states, i.e., crystalline, amorphous or liquid, has been an extensively studied material of geophysical relevance, owing to its importance to the fact that it is a high pressure analog of SiO_2. Theoretically and experimentally it has been shown that amorphous SiO_2 transforms from a low density amorphous phase (LDA) (4 coordinated) to a high density amorphous phase (HDA) (6 coordinated) via an intermediate state having an average coordination of 5 (refs 76–80). Though several experiments showed a LDA to HDA transformation in vitreous GeO_2 (refs 81–84), Guthrie et al.[85] seemed to suggest that the coordination change in Ge–O is not a continuous change from 4–6 but proceeds via a plateau of pure pentahedrally coordinated Ge–O between 6–10 GPa.

This was somehow not convincing as our studies on amorphous quartz had shown that the coordination increases from 4 to 6 (ref. 80). Also as the atomic movements can be followed in an MD calculation, the high pressure amorphous phase of SiO_2 could be visualized as a mixture of 4, 5 and 6 coordinated Si–O. To understand these[85] unusual experimental results we carried out MD calculations on vitreous GeO_2 and did not find any high pressure region in which Ge–O showed a purely pentahedrally coordinated state (Figure 10)[86]. Subsequent to our studies[86] their have been several theoretical and experimental studies like EXAFS, inelastic X-ray scattering, and neutron diffraction, but none of them supported the presence of a pure pentahedral state of Ge–O thus vetting our results[87–92]. Since collection of good data of vitreous samples is experimentally challenging, and analysis of this data is non-trivial, specially if it is noisy, it is possible that the extracted coordination of Ge–O from earlier X-ray and neutron diffraction data may not have been reliable[85]. Recently some very good diffraction experiments by Konoa et al.[93] have shown that in vitreous samples of GeO_2, the Ge–O coordination increases to 7.4 at 90 GPa.

Bismuth ferrite and $YLiF_4$

The examples in this section demonstrate how both first principles calculations and rietveld least square refinement methods can be used to arrive at the structure of new high pressure phases. Mostly structure solution at high pressure is not very easy as the powder diffraction data may be limited or weak, and in addition, there may be several competing structures. Most of the refinement programmes start with a model structure and carry out a least square refinement with respect to the collected diffraction data. However, if the initial structural model is not very close to the structure of the high pressure phase, the refinement may result in a local minima rather than a global minima. We may end up with strained bonds or altogether erroneous structures. Unlike first principles calculations, these refinement programmes do not factor in the energetics involved, in the changing of the chemical bonds or force fields with pressure (To mitigate this problem to some extent we incorporate constraints into the refinement model). This often leads to structure solutions which may in reality have no stability. To overcome this problem, the results from rietveld refinement were interweaved with first principle studies to arrive at realistic structure solutions for these compounds. In this method some initial structure model is determined with the help of rietveld refinement methods. The coordinates from these refinements are then used as the starting coordinates in ab initio calculations and the structures are allowed to relax and stabilize by minimizing the interatomic forces. Once again the stabilized structure is used as the initial model for the rietveld refinement. This process can be repeated till a satisfactory structure of the high pressure phase is determined.

Using this methodology, the high pressure structure of both bismuth ferrite[94] and erbium lithium fluoride was determined successfully[95]. $BiFeO_3$ is a multiferroic material with a rhombohedraly distorted perovskite structure (R3c). In literature there were several[96–100] varied reports which showed, that $BiFeO_3$ transforms from R3c to Pnma, via a monoclinic phase or two orthorhombic phases. With the help of our combined theoretical and experimental approach we determined that the first high
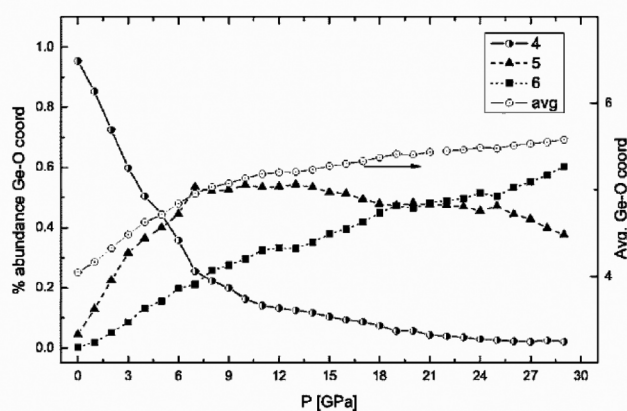

Figure 10. Average coordination of Ge–O and variation of abundance of Ge–O coordination as a function of pressure. (Reproduced from ref. 89 with copyright permission from APS).

pressure phase of $BiFeO_3$ is orthorhombic $P222_1$ and not $C2/m$ (ref. 94).

Similarly in $ErLiF_4$ a scheelite structured fluoride, the first high pressure phase could be fitted to the well-known fergusonite phase. However, since the diffraction contrast between light elements like 'Li' and 'F' and heavy metals like 'Er' is large in the X-ray diffraction data, the atomic coordinates of the lighter atoms could not be determined with high precision. To get better positions of the lighter elements, *ab initio* calculations were carried out, wherein the configuration energy was minimized by relaxing the bond strains. Thus the refined structure of the fergusonite phase could be determined[95].

Porous silicon

Both bulk and nano-silicon, due to their wonderful properties have a lot of technological importance, specially in the electronics sector. Bulk silicon is known to transform to several dense phases with similar or higher coordination like β-tin, primitive hexagonal (ph), orthorhombic (Cmca), hexagonal close packed (hcp) and face centred cubic (fcc) at high pressures[101–108]. Though, Tolbert *et al.*[105] showed that 10–50 nm silicon did not transform to the beta tin or orthorhombic phases but directly transformed to the 'ph' phase, silicon nano wires showed the same sequence of phase transition as observed in bulk. However, it was a bit surprising that 5 nm silicon particles embedded in porous silicon amorphized rather than undergoing transformations to crystalline phases[109]. As silicon has a negative claperyon slope these results were rationalized in terms of pseudomelting[109]. However, our X-ray diffraction studies at an intense synchrotron source Spring8, showed that 5 nm silicon particles embedded in porous silicon, transformed directly to the 'ph' phase and amorphized only on release of pressure[110]. This discrepancy between earlier results and our results was because the earlier authors had erroneously concluded amorphization based on Raman results. (The 'ph' phase has no Raman active modes and hence appears amorphous)

Interestingly the amorphous to 'ph' phase transformation showed recyclability. It is known that when a bulk material is suddenly decompressed, or a liquid is suddenly cooled the metastable amorphous phase can get trapped. However, in the present case, even on slow release of pressure, a nano cluster of silicon was transforming from the crystalline 'ph' structure to an amorphous structure, indicating that this transformation was not kinetics-dependent. This was also confirmed with the help of *ab initio* calculations, wherein stability of small clusters of silicon having the beta tin phase, amorphous phase and the diamond phase (Figure 11) was examined at ambient pressure and the amorphous structure was found to be the most stable with minimum total energy[110]. Also reversible crystal-to-crystal transformations can be un-

derstood as a collective reordering of the atoms from one phase to another as there exists long range order. However, in reversible disordered solid to crystal transformation it is difficult to imagine a simple transformation path. The reversible transformation from amorphous to 'ph' can be explained if the energy barriers for formation of other crystalline phases are always larger than that of the 'ph' phase. Even though β-Sn and Imma phases have a region of stability close to that of the 'ph' phase, invoking the thermodynamical model based on the random nucleation and growth process we showed that beyond 5 GPa, both the critical diameter for nucleation and the nucleation work are lower for the 'ph' phase. This could lead to a higher nucleation rate of the 'ph' phase and hence its preferential crystallization[111]. Even model calculations, where a cluster of 'ph' silicon was surrounded by 28,000 liquid atoms, and the liquid was treated classically but the cluster was treated by *ab initio* methods, showed that at ambient pressure the 'ph' cluster became disordered as shown in Figure 12. Thus with the help of both theory and experiments we could show that amorphous state is the stable state at ambient conditions in nanosilicon and due to increased nucleation rate of 'ph' phase, viz. beta tin and Imma, in nanocrystals, nano-amorphous silicon crystallizes to the 'ph' phase on application of pressure.

Yttrium chromate

All high pressure studies on bulk zircon and zircon structured materials have shown that they transform from the zircon to the scheelite structure at high pressure[112,113]. Kusaba *et al.*[114] had suggested that the angle of intersection between the *a* and *b* direction changes abruptly from
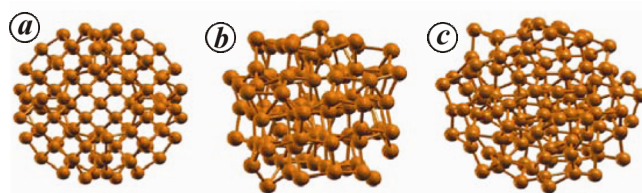

Figure 11. Cluster of silicon at ambient pressure. *a*, Diamond phase; *b*, Relaxed beta tin phase; *c*, Amorphous phase.
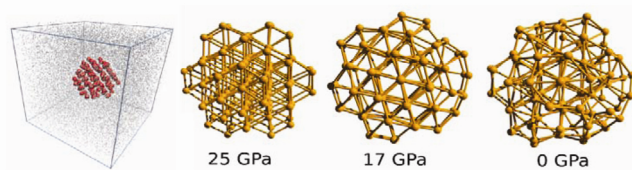

Figure 12. Silicon cluster in the 'ph' phase at different pressures and surrounded by atoms depicting a liquid which was treated classically (reproduced from thesis of K. V. Shanavas).
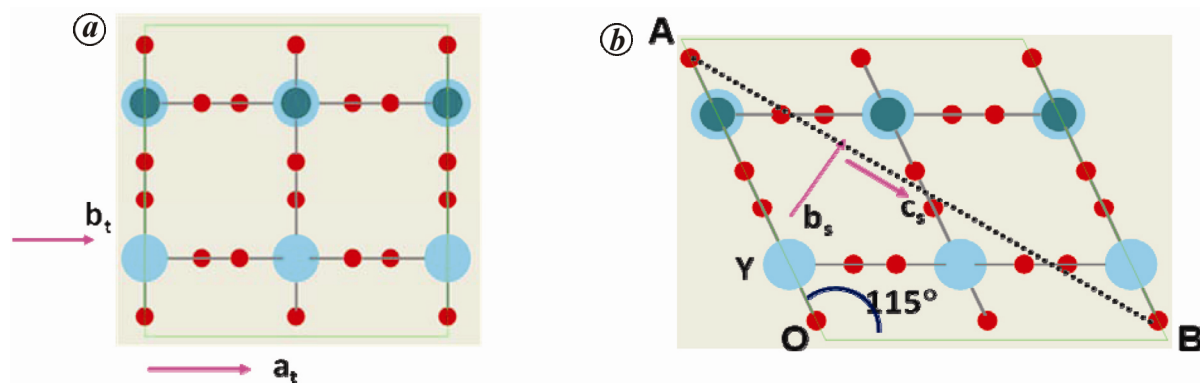
Figure 13. *a*, The basal *ab* plane of the zircon phase of YCrO$_4$. The yttrium, oxygen and chromium atoms are shown in blue, red and green colours. *b*, This shows the distortion in the basal plane which will lead to the scheelite phase. The *b* and *c* axis of the scheelite phase have been shown in the figure as b_s and c_s.

90° to 115°, due to the shear in the basal plane, resulting in the zircon to scheelite phase transformation (Figure 13). However, if the angle changes smoothly during transformation then the intermediate states have to have a monoclinic symmetry and cannot satisfy the tetragonal symmetry. Based on group-subgroup analysis, some authors have suggested that the transformation path of zircon to scheelite phase transformation is $I4_1/amd \rightarrow Fddd \rightarrow C2/c \rightarrow I4_1/a$ (ref. 115), but none of the experimental studies could show the presence of the intermediate monoclinic phase. Since all these studies were on bulk materials, and it is known that certain transformations are possible when working in the nano-regime due to altered surface and total energies of nanosamples we decided to explore the presence of monoclinic phase in nanoyttrium chromate. Our conclusions from the experimental data, on the presence of the intermediate monoclinic phase, were based on the interpretations from a close analysis of the full width half maxima of the diffraction peaks[116]. However, since the diffraction peaks were not well resolved and the differences were very subtle, there was a need to verify if indeed the intermediate phase existed. Total energy calculations were carried out using *ab initio* methods and it was observed that monoclinic phase indeed had lower energy than the scheelite phase, thus giving us confidence that the monoclinic phase could be stabilized under favourable conditions[116].

Lanthanum hafnate

Pyrochlores are important materials in the nuclear industry, as, due to their retention of actinides and lanthanides, they can be used for fixation of nuclear waste[117–119]. Lanthanum hafnate, a pyrochlore, is also a potential candidate for usage as a nuclear encapsulant, specially as one of its constituents hafnium, is a neutron absorber. However, to understand its usability we have to be sure that it has a stable structure and has long term mechanical and chemical durability with respect to natural calamities like earthquakes, etc. Our high pressure experimental studies indicate that it dissociates into its constituent oxides at high pressure. To understand the dissociation of lanthanum hafnate at high pressures, *ab initio* calculations were carried out. These studies showed that the constituent oxides (HfO$_2$ and La$_2$O$_3$), indeed, had a lower free energy when compared to lanthanum hafnate, at high pressure, thus explaining the high pressure dissociation of this pyrochlore. Thus it can be seen that with the help of both experimental and theoretical studies we were able to conclude that lanthanum hafnate may not be suitable as a nuclear encapsulant[120].

Organic molecular solids

Oxalic acid dihydrate is the simplest dicarboxylic acid complex and has a very short hydrogen bond between water and oxalic acid at ambient pressure[121]. Proton dynamics across such short, nearly symmetric hydrogen bonds could lead to several bio-geological processes[122–125]. Proton transfer between water and oxalic acid across this short hydrogen bond has not been observed at ambient or low temperature. However, our high pressure IR studies (emergence of the O–H mode at ~3100 cm^{-1}) clearly showed the presence of hydronium ion (H$_3$O) beyond 2 GPa, indicating proton migration from oxalic acid to water[126]. These experimental studies were vetted with *ab initio* calculations by A. K. Verma which clearly showed the transfer of proton, along the O–H–O bond, at very low pressures. However, here it is worth mentioning that with the standalone IR results it would have been difficult to arrive at this conclusion, as the IR mode present at 3100 cm^{-1} which is a definitive signature of the hydronium ion, is actually a very broad band and can be easily mistaken to be a part of the background if the fitting is not done properly. Even glycinium oxalate (GO), the simplest amino acid−carboxylic acid complex, has very

short hydrogen bonds. Our high pressure IR and Raman studies have shown a dynamic sharing of the proton between the two semioxalate units of glycinium oxalate, thus mimicking a symmetric hydrogen bond state. These results were corroborated with the help of *ab initio* calculations which showed that the probability of crossing the midpoint between the oxalates increased with pressure[127].

Conclusions

From this article it can be seen that application of high pressure brings about a myriad of exciting changes. It can lead to crystal-to-crystal changes or could lead to amorphization. There are studies where we have seen insulator to metal transitions and also piezochromic behaviour at high pressure[8]. Specially, with the pressure limits being pushed to terapascals[51] with the help of the small DAC in the lab and with better and better diagnostic equipment we can expect to see major advances in the field of high pressure science.

1. Glenzer, S. H. *et al*., Matter under extreme conditions experiments at the Linac Coherent Light Source. *J. Phys. B: At. Mol. Opt. Phys*., 2016, **49**, 092001–092027.
2. Lange, K. K., Tellgren, E. I., Hoffmann, M. R. and Helgaker, T., A paramagnetic bonding mechanism for diatomics in strong magnetic fields. *Science*, 2012, **337**, 327–331.
3. https://en.wikipedia.org/wiki/Orders_of_magnitude_(pressure)
4. Fox-Skelly, J., 2015; http://www.bbc.com/earth/story/20150129-life-at-the-bottom-of-the-ocean
5. Hazen, R. M., Boctor, N., Brandes, J. A., Cody, G. D., Hemley, R. J., Sharma, A. and Yoder Jr, H. S., High pressure and the origin of life. *J. Phys. Cond. Matter*., 2002, **14**, 11489–11494.
6. Anurag, S., Scott, J. H., Cody, G. D., Fogel, M. L., Hazen, R. M., Hemley, R. J. and Huntress, W. T., Microbial activity at gigapascal pressures. *Science*, 2002, **295**, 1514–1516.
7. Badding, J. V., Parker, L. J. and Nesting, D. C., High pressure synthesis of metastable materials. *J. Solid State Chem*., 1995, **117**, 229–235.
8. Ghalsasi, P., Garg, N., Deo, M. N., Garg, A., Mande, H., Ghalsasi, P. and Sharma, S. M., The role of Jahn–Teller distortion in insulator to semiconductor phase transition in organic–inorganic hybrid compound (p-chloroanilinium)₂CuCl₄ at high pressure. *Phys. Chem. Chem. Phys*., 2015, **17**, 32204–32210.
9. Bundy, F. P., Hall, H. T., Strong, H. M. and Wentorf, R. H., Man-made diamonds. *Nature*, 1955, **176**, 51–55.
10. Wentorf, H. R. J., Cubic form of boron nitride. *Chem. Phys*., 1957, **26**, 956.
11. Irifune, T., Kurio, A., Sakamoto, S., Inoue, T. and Sumiya, H., Materials: ultrahard polycrystalline diamond from graphite. *Nature*, 2003, **421**, 599–600.
12. Sumiya, H. and Irfune, T., Microstructure and mechanical properties of high-hardness nano-polycrystalline diamonds. *Sci. Tech. Rev*., 2008, **66**, 85–92.
13. Dubrovinskaia, N., Dubrovinsky, L., Langenhorst, F., Jacobsen, S. and Liebske, C., Nanocrystalline diamond synthesized from C60. *Diam. Relat. Mater*., 2005, **14**, 16–22.
14. Irifune, T., Isobe, F. and Shinmei, T., A novel large-volume Kawai-type apparatus and its application to the synthesis of sintered bodies of nano-polycrystalline diamond. *Phys. Earth Planet*., 2014, **228**, 255–261.
15. Sumiya, H. and Irifune, T., Hardness and deformation microstructures of nano-polycrystalline diamonds synthesized from various carbons under high pressure and high temperature. *J. Mater. Res*., 2007, **22**, 2345–2351.
16. McWilliams, R. Stewart, Allen Daltona, D., Konôpkováf, Z., Mahmooda, M. F. and Goncharova, A. F., Opacity and conductivity measurements in noble gases at conditions of planetary and stellar interiors. *Proc. Natl. Acad. Sci*., 2015, **112**, 7925–7930.
17. Bergeron, P., Saumon, D. and W. F., New model atmospheres for very cool white-dwarfs with mixed H/He and pure He compositions. *Astrophys. J*., 1995, **443**, 764–779.
18. Celliers, P. M. *et al*., Insulator-to-conducting transition in dense fluid helium. *Phys. Rev. Lett*., 2010, **104**, 184503–184504.
19. Pan, Y., Inam, F., Zhang, M. and Da, D., Atomistic origin of urbach tails in amorphous silicon. *Phys. Rev. Lett*., 2008, **100**, 206403–206404.
20. Tomoaki Kubo, Takumi Kato, Yuji Higo, and Ken-ichi Funakoshi, Curious kinetic behavior in silica polymorphs solves seifertite puzzle in shocked meteorite. *Sci. Adv*., 2015, **1**, e1500075.
21. Millot, M. *et al*., Shock compression of stishovite and melting of silica at planetary interior conditions. *Science*, 2015, **347**, 418–420.
22. Niu, H. Y., Oganov, A. R., Chen, X. Q. and Dz, L., Prediction of novel stable compounds in the Mg–Si–O system under exoplanet pressures. *Sci. Rep*., 2015, **5**, 18347–18356.
23. Wang, H., Zeuschner, J., Eremets, M., Troyan, I. and Williams, J., Stable solid and aqueous H₂CO₃ from CO₂ and H₂O at high pressure and high temperature. *Sci. Rep*., 2016, **6**, 19902–19910.
24. Bykova, E. *et al*., Structural complexity of simple Fe₂O₃ at high pressures and temperatures. *Nature Commun*., 2016, **7**, 10661–10669.
25. Ramaker, D. E., Kumar, L. and Harris, F. E., Exact-exchange crystal Hartree–Fock calculations of molecular and metallic hydrogen and their transitions. *Phys. Rev. Lett*., 1975, **34**, 812–816.
26. Friedli, C. and Ashcroft, N. W., Combined representation method for use in band-structure calculations: Application to highly compressed hydrogen. *Phys. Rev. B*, 1977, **16**, 662–672.
27. Wigner, E. and Huntington, H. B., On the possibility of a metallic modification of hydrogen. *J. Chem. Phys*., 1935, **3**, 764–770.
28. Conover, E., The pressure is on to make metallic hydrogen. *Sci. News*, 2016, **190**, 18.
29. Mazzola, G., Yunoki, S. and Sorella, S., Unexpectedly high pressure for molecular dissociation in liquid hydrogen by electronic simulation. *Nat. Commun*., 2014, **5**, 3487–3493.
30. Cohen, R. E., Naumov, I. I. and Hemley, R. J., Electronic excitations and metallization of dense solid hydrogen. *Proc. Natl. Acad. Sci*., 2013, **110**, 13757–13762.
31. Azadi, S. and Kühne, T. D., Absence of metallization in solid molecular hydrogen. *JETP Lett*., 2012, **95**, 449–453.
32. Eremets, M. I. and Troyan, I. A., Conductive dense hydrogen. *Nature Mater*., 2011, **10**, 927–931.
33. Drozdov, A. P., Eremets, M. I., Troyan, I. A., Ksenofontov, V. and Shylin, S. I., Conventional superconductivity at 203 kelvin at high pressures in the sulfur hydride system. *Nature*, 2015, **525**, 73–76.
34. Ge, Y., Zhang, F. and Yao, Y., First-principles demonstration of superconductivity at 280 K in hydrogen sulfide with low phosphorus substitution. *Phys. Rev. B*, 2016, **93**, 224513–224522.
35. Zhang, W. *et al*., Unexpected stable stoichiometries of sodium chlorides. *Science*, 2013, **342**, 1502–1505.
36. Li, Y. L. *et al*., Investigation of exotic stable calcium carbides using theory and experiment. *Nature Commun*., 2015, **6**, 6974–6983.
37. Masson, P., Tonello, C. and Balny, C., High-pressure biotechnology in medicine and pharmaceutical science. *J. Biomed. Biotechnol*., 2001, **1**, 85–88.
38. Evlyukhin, E., Museur, L., Traore, M., Perruchot, C., Zerr, A. and Kanaev, A., Materials: High-pressure-Ramp-induced

ultrafast polymerization of 2-(hydroxyethyl)methacrylate. *Sci. Rep.*, 2015, **5**, 18244–18253.

39. Chiarello, G. L., Aguirre, M. H. and Selli, E., Hydrogen production by photocatalytic steam reforming of methanol on noble metal-modified TiO₂. *J. Catal.*, 2010, **273**, 182–190.

40. Patterson, M. F., McKay, A. M., Connolly, M. and Linton, M., The effect of high hydrostatic pressure on the microbiological quality and safety of carrot juice during refrigerated storage. *Food Microbiol.*, 2012, **30**, 205–212.

41. Shahbaz, H. M. *et al.*, Combination of TiO₂–UV photocatalysis and high hydrostatic pressure to inactivate bacterial pathogens and yeast in commercial apple juice. *Food Bioprocess Technol.*, 2016, **9**, 182–192.

42. Horie, Y., Kimura, K. and Hori, K., Development of a new fruit processing method by high hydrostatic pressure. *J. Agric. Chem. Soc. Jpn.*, 1991, **65**, 1469.

43. Yaldagard, M., Seyed Ali Mortazavi and Tabatabaie, F., The principles of ultra high pressure technology and its application in food processing/preservation: a review of microbiological and quality aspects. *Afr. J. Biotechnol.*, 2008, **7**, 2739–2767.

44. Chen, C.-T. A., *Oceanography, Carbonate Chemistry of the Oceans*, vol. 1.

45. Jayaraman, A., Diamond anvil cell and high pressure physical investigations. *Rev. Mod. Phys.*, 1983, **55**, 65–108.

46. Eremets, M. I., *High Pressure Experimental Methods*, Oxford University Press, 1996.

47. Rahman, A., Correlations in the motion of atoms in liquid argon. *Phys. Rev. B.*, 1964, **136**, A405–A411.

48. Car, R. and Parrinello, M., Unified approach for molecular dynamics and density functional theory. *Phys. Rev. Lett.*, 1985, **55**, 2471–2475.

49. Allen, M. P. and Tildesley, D. J., *Computer Simulation of Liquids*, Oxford University Press, 1987.

50. Glass, C. W., Oganov, A. R. and Hansen, N., USPEX – evolutionary crystal structure prediction. *Comp. Phys. Commun.*, 2006, **175**, 713–720.

51. Dubrovinskaia, N. *et al.*, Terapascal static pressure generation with ultrahigh yield strength nanodiamond. *Sci. Adv.*, 2016, **2**, e1600341–e1600353.

52. Katsura, T. *et al.*, A large-volume high-pressure and high-temperature apparatus for *in situ* X-ray observation. *Phys. Earth Planet. Int.*, 2004, **143**, 497–506.

53. Ito, E. *et al.*, Pressure generation and investigation of the post-perovskite transformation in MgGeO₃ by squeezing the Kawai-cell equipped with sintered diamond anvils. *Earth Planet. Sci. Lett.*, 2010, **293**, 84–89.

54. Evans, W. J., Yoo, C.-S., Lee, G. W., Cynn, H., Lipp, M. J. and Visbeck, K., Dynamic diamond anvil cell (dDAC): A novel device for studying the dynamic-pressure properties of materials. *Rev. Sci. Inst.*, 2007, **78**, 073904–073910.

55. Bhatt, H., Murli, C., Garg, N., Deo, M. N., Chitra, R., Choudhury, R. R. and Sharma, S. M., High pressure phase transformations in bis(glycinium)oxalate – an infrared absorption study. *Chem. Phys. Lett.*, 2012, **532**, 57–62.

56. Klotz, S., Chervin, J.-C., Munsch, P. and Le Marchand, G., Hydrostatic limits of 11 pressure transmitting media. *J. Phys. D: Appl. Phys.*, 2009, **42**, 075413–075420.

57. Sekar, M., Sanjay Kumar, N. R., Ch, P., Sahu, Chandra Shekar, N. V. and Subramanian, N., Cryogenic gas loading in a Mao-Bell-type diamond anvil cell for high pressure-high temperature investigations. *Rev. Sci. Instrum.*, 2008, **79**, 076103–076106.

58. Mao, H. K., Xu, J. and Bell, P. M., Calibration of the ruby pressure gauge to 800 kbar under quasi-hydrostatic conditions. *J. Geophys. Res.*, 1986, **91B**, 4673–4676.

59. Hemley, R. J., Zha, C. S., Jephcoat, A. P., Mao, H. K. and Finger, L. W., X-ray diffraction and equation of state of solid neon to 110 GPa. *Phys. Rev. B*, 1989, **39**, 11820–11827.

60. Silvera, I. F., Chijioke, A. D., Nellis, W. J., Soldatov, A. and Tempere, J., Calibration of the ruby pressure scale to 150 GPa. *Phys. Stat. Sol.*, 2007, **244**, 460–467.

61. Chijioke, A. D., Nellis, W. J., Soldatov, A. and Silvera, I. F., The ruby pressure standard to 150 GPa. *J. Appl. Phys.*, 2005, **98**, 114905–114914.

62. Dorogokupets, P. I. and Oganov, A. R., Ruby, metals, and MgO as alternative pressure scales: a semiempirical description of shock-wave, ultrasonic, X-ray, and thermochemical data at high temperatures and pressures. *Phys. Rev. B*, 2007, **75**, 024115–024131.

63. Dewaele, A., Loubeyre, L. P. and Mezouar, M., Equations of state of six metals above 94 GPa. *Phys. Rev. B*, 2004, **70**, 094112–094120.

64. Pandey, K. K., Poswal, H. K., Mishra, A. K., Dwivedi, A., Vasanthi, R., Garg, N. and Sharma, S. M., Energy dispersive X-ray diffraction beamline at Indus-2 synchrotron source. *Pramana*, 2013, **80**, 607–619.

65. Kruger, M. B. and Jeanloz, R., Memory glass: an amorphous material formed from aluminum phosphate. *Science*, 1990, **249**, 647.

66. Sankaran, H., Sharma, S. M., Sikka, S. K. and Chidambaram, R., Pressure induced amorphization of AlPO₄. *Pramana – J. Phys.*, 1990, **35**, 177–180.

67. Somayazulu, M. S., Garg, N., Sharma, S. M. and Sikka, S. K., Search for a precursor crystal-to-crystal phase transition to amorphization in α-GeO₂ and α-AlPO₄ under pressure. *Pramana – J. Phys.*, 1994, **43**, 1–9.

68. Tse, J. S. and Klug, D. D., Structural memory in pressure-amorphized AlPO₄. *Science*, 1992, **255**, 1559–1561.

69. Chaplot, S. L. and Sikka, S. K., Molecular-dynamics simulation of pressure-induced crystalline-to-amorphous transition in some corner-linked polyhedral compounds. *Phys. Rev. B*, 1993, **47**, 5710–5714.

70. Gillet, P., Badro, J., Varrel, B. and McMillan, P. F., High-pressure behavior in α-AlPO₄: amorphization and the memory-glass effect. *Phys. Rev. B*, 1995, **51**, 11262–11270.

71. Murli, C., Sharma, S. M., Kulshreshtha, S. K. and Sikka, S. K., High pressure study of phase transitions in alpha-FePO₄. *Pramana – J. Phys.*, 1997, **49**, 285–291.

72. Pasternak, M. P. *et al.*, Pressure-induced concurrent transformation to an amorphous and crystalline phase in berlinite-type FePO₄. *Phys. Rev. Lett.*, 1997, **79**, 4409–4412.

73. Garg, N. and Sharma, S. M., A molecular dynamical investigation of high pressure phase transformations in berlinite (alpha-AlPO₄). *J. Phys. Condens. Matter*, 2000, **12**, 375–397.

74. Sharma, S. M., Garg, N. and Sikka, S. K., High-pressure X-ray-diffraction study of α-AlPO₄. *Phys. Rev. B*, 2000, **62**, 8824–8827.

75. Pellicer-Porres, J., Saitta, A. M., Polian, A., Itie, J. P. and Hanfland, M., Six-fold-coordinated phosphorus by oxygen in AlPO₄ quartz homeotype under high pressure. *Nature Mat.*, 2007, **6**, 698–702.

76. Tse, J. S. and Klug, D. D., Mechanical instability of α-quartz: A molecular dynamics study. *Phys. Rev Lett.*, 1991, **67**, 3559–3562.

77. Somayazulu, M. S., Sharma, S. M., Garg, N., Chaplot, S. L. and Sikka, S. K., The behaviour of alpha-quartz and pressure-induced SiO₂ glass under pressure: a molecular dynamical study. *J. Phys. Condens. Matter.*, 1993, **5**, 6345–6356.

78. Sato, T. and Funamori, N., Six-fold-coordinated amorphous polymorph of SiO₂ under high pressure. *Phys. Rev. Lett.*, 2008, **101**, 255502–255505.

79. Sato, T. and Funamori, N., High-pressure structural transformation of SiO₂ glass up to 100 GPa. *Phys. Rev. B*, 2010, **82**, 184102–184105.

80. Wu, M., Liang, Y., Jiang, J.-Z. and Tse, J. S., Structure and properties of dense silica glass. *Sci. Rep.*, 2012, **2**, 398–404.

81. Itie, J. P., Polian, A., Calas, G., Petiau, J., Fontaine, A. and Tolentino, H., Pressure-induced coordination changes in crystalline and vitreous GeO_2. *Phys. Rev. Lett.*, 1989, **63**, 398–401.

82. Polsky, H., Smith, K. H. and Wolf, G. H., Effect of pressure on the absolute Raman scattering cross section of SiO_2 and GeO_2 glasses. *J. Non-Cryst. Solids*, 1999, **248**, 159–168.

83. Grimsditch, M., Bhadra, R. and Meng, Y., Brillouin scattering from amorphous materials at high pressures. *Phys. Rev. B*, 1988, **38**, 7836–7838.

84. Meade, C., Hemley, R. J. and Mao, H. K., High-pressure X-ray diffraction of SiO_2 glass. *Phys. Rev. Lett.*, 1992, **69**, 1387–1390.

85. Guthrie, M. *et al.*, Formation and structure of a dense octahedral glass. *Phys. Rev. Lett.*, 2004, **93**, 115502–115505.

86. Shanavas, K. V., Garg, N. and Sharma, S. M., Classical molecular dynamics simulations of behavior of GeO_2 under high pressures and at high temperatures. *Phys. Rev. B*, 2006, **73**, 094120–094132.

87. Baldini, M., Aquilanti, G., Mao, H-K., Yang, W., Shen, G., Pascarelli, S. and Mao, W. L., High-pressure EXAFS study of vitreous GeO_2 up to 44 GPa. *Phys. Rev. B*, 2010, **81**, 024201–024207.

88. Hong, X., Newville, M., Duffy, T. S. Sutton, S. R. and Rivers, M. L., X-ray absorption spectroscopy of GeO_2 glass to 64 GPa. *J. Phys.: Condens. Matter*, 2014, **26**, 035104–035113.

89. Marrocchelli, D., Salanne, M. and Madden, P. A., High-pressure behaviour of GeO_2: a simulation study. *J. Phys.: Condens. Matter*, 2010, **22**, 152102–152110.

90. Lelong, G., Cormier, L., Ferlat, G., Giordano, V., Henderson, G. S., Shukla, A. and Calas, G., Evidence of fivefold-coordinated Ge atoms in amorphous GeO_2 under pressure using inelastic X-ray scattering. *Phys. Rev. B*, 2012, **85**, 134202–134207.

91. Cunsolo, A. *et al.*, Signature of a polyamorphic transition in the THz spectrum of vitreous GeO_2. *Sci. Rep.*, 2015, **5**, 14996–15005.

92. Wezka, K. *et al.*, Mechanisms of network collapse in GeO_2 glass: high-pressure neutron diffraction with isotope substitution as arbitrator of competing models. *J. Phys.: Condens. Matter.*, 2012, **24**, 502101–502110.

93. Konoa, Y. *et al.*, Ultrahigh-pressure polyamorphism in GeO_2 glass with coordination number >6. *Proc. Natl. Acad. Sci.*, 2016, **113**, 3436–3441.

94. Mishra, A. K., Shanavas, K. V., Poswal, H. K., Mandal, B. P., Garg, N. and Sharma, S. M., Pressure induced phase transitions in multiferroic $BiFeO_3$. *Solid State Commun.*, 2013, **154**, 72–76.

95. Garg, N., Mishra, A. K., Poswal, H. K., Tyagi,, A. K. and Sharma, S. M., High pressure phase transitions in scheelite structured fluoride: $ErLiF_4$. *J. Solid State Chem.*, 2015, **229**, 164–172.

96. Haumont, R., Bouvier, P., Pashkin, A., Rabia, K., Frank, S., Dkhil, B., Crichton, W. A., Kuntscher, C. A. and J. K., Effect of high pressure on multiferroic $BiFeO_3$. *Phys. Rev. B*, 2009, **79**, 184110–184120.

97. Gavriliuk, A. G., Struzhkin, V. V., Lyubutin, I. S., Ovchinnokov, S. G., Hu, M. Y. and Chow, P., Another mechanism for the insulator-metal transition observed in Mott insulators. *Phys. Rev. B*, 2008, **77**, 155112–155118.

98. Ravindran, P., Vidya, R., Kjekshus, A., Fjellvag, H. and Eriksson, O., Theoretical investigation of magnetoelectric behavior in $BiFeO_3$. *Phys. Rev. B.*, 2006, **74**, 224412–224418.

99. Vazquez, O. E. G. and Iniguez, J., Pressure-induced structural, electronic, and magnetic effects in $BiFeO_3$. *Phys. Rev. B*, 2009, **79**, 064102–064106.

100. Belik, A. A., Yusa, H., Hirao, N., Ohishi, Y. and Takayama-Muromachi, E., Structural properties of multiferroic $BiFeO_3$ under hydrostatic pressure. *Chem. Mater.*, 2009, **21**, 3400–3405.

101. Olijynk, H., Sikka, S. K. and Holzaphel, W. B., Structural phase transitions in Si and Ge under pressures up to 50 GPa. *Phys. Lett. A*, 1984, **103A**, 137–140.

102. McMillan, P. F., Wilson, M., Wilding, M. C., Daisenberger, D., Mezouar, M. and Greaves, G. N., Polyamorphism and liquid–liquid phase transitions: challenges for experiment and theory. *J. Phys.: Condens. Mater*, 2007, **19**, 415101–415142.

103. Jamieson, J. C., Crystal structures at high pressures of metallic modifications of silicon and germanium. *Science*, 1963, **139**, 762–764.

104. Wentorf, R. H. and Kasper, J. H., Two new forms of silicon. *Science*, 1963, **139**, 338–339.

105. Tolbert, S. H., Herhold, A. B., Brus, L. E. and Alivisatos, A. P., Pressure-induced structural transformations in Si nanocrystals: surface and shape effects. *Phys. Rev. Lett.*, 1996, **76**, 4384–4388.

106. Tolbert, S. H. and Alivisatos, A. P., High-pressure structural transformations in semiconductor nanocrystals. *Annu. Rev. Phys. Chem.*, 1995, **46**, 595–626.

107. Poswal, H. K. *et al.*, Pressure-induced structural phase transformations in silicon nanowires. *J. Nanosci. Nanotech.*, 2005, **5**, 729–732.

108. Domnich, V. and Gogotsi, Y., Phase transformations in silicon under contact loading. *Rev. Adv. Mat. Sci.*, 2002, **3**, 1–36.

109. Deb, S. K., Wilding, M. C., Somayazulu, M. and McMillan, P. F., Pressure-induced amorphization and an amorphous–amorphous transition in densified porous silicon. *Nature*, 2001, **414**.

110. Garg, N., Pandey, K. K., Shanavas, K. V., Betty, C. A. and Sharma, S. M., Memory effect in low-density amorphous silicon under pressure. *Phys. Rev. B*, 2011, **83**, 115202–115208.

111. Pandey, K. K., Garg, N., Shanavas, K. V., Sharma, S. M. and Sikka, S. K., Pressure induced crystallization in amorphous silicon. *J. App. Phys.*, 2011, **109**, 113511–113518.

112. Marques, M., Florez, M., Recio, J. M., Gerward, L. and Olsen, J. S., Structure and stability of $ZrSiO_4$ under hydrostatic pressure. *Phys. Rev. B*, 2006, **74**, 014104–014113.

113. Wang, X., Loa, I., Syassen, K., Hanfland, M. and Ferrand, B., Structural properties of the zircon- and scheelite-type phases of YVO_4 at high pressure. *Phys. Rev. B*, 2004, **70**, 064109–064115.

114. Kusaba, K., Yagi, T., Kikuchi, M. and Syono, Y., Structural considerations on the mechanism of the shock-induced zircon-scheelite transition in $ZrSiO_4$. *J. Phys. Chem. Solids*, 1986, **47**, 675–679.

115. Smirnov, M. B., Mirgorodsky, A. P., Kazimirov, V. Y. and Guinebretière, R., Bond-switching mechanism for the zircon-scheelite phase transition. *Phys. Rev. B*, 2008, **78**, 094109–094120.

116. Mishra, A. K., Garg, N., Pandey, K. K., Shanavas, K. V., Tyagi, A. K. and Sharma, S. M., Zircon-monoclinic-scheelite transformation in nanocrystalline chromates. *Phys. Rev. B*, 2010, **81**, 104109–104115.

117. Sickafus, K. E. *et al.*, Radiation tolerance of complex oxides. *Science*, 2000, **289**, 748–751.

118. Mandal, B. P., Garg, N., Sharma, S. M. and Tyagi, A. K., Solubility of ThO_2 in $Gd_2Zr_2O_7$ pyrochlore: XRD, SEM and Raman spectroscopic studies. *J. Nucl. Mater.*, 2009, **392**, 95–99.

119. Ewing, R. C., Weber, W. J. and Lian, J., Nuclear waste disposal – pyrochlore $A_2B_2O_7$...: nuclear waste form for the immobilization of plutonium and 'minor' actinides. *J. Appl. Phys.*, 2004, **95**, 5949–5971.

120. Garg, N. *et al.*, Decomposition of lanthanum hafnate at high pressures. *Phys. Rev. B*, 2008, **77**, 214105–214113.

121. Mohacĕk-Grosĕv, V., Grdadolnik, J., Stare, J. and Hadži, D., Identification of hydrogen bond modes in polarized Raman spectra of single crystals of α-oxalic acid dihydrate. *Raman Spectrosc.*, 2009, **40**, 1605–1614.

122. Berkelbach, T. C., Lee, H.-S. and Tuckerman, M. E., Concerted hydrogen-bond dynamics in the transport mechanism of the hydrated proton: a first-principles molecular dynamics study. *Phys. Rev. Lett.*, 2009, **103**, 238302–238306.

123. Hassanali, A., Giberti, F., Cuny, J., Kühne, T. D. and Parrinello, M., Proton transfer through the water gossamer. *Proc. Natl. Acad. Sci.*, 2013, **110**, 13723–13728.

124. Heyden, M. and Tobias, D. J., Spatial dependence of protein-water collective hydrogen-bond dynamics. *Phys. Rev. Lett.*, 2013, **111**, 218101–218105.

125. Sigala, P. A. *et al.*, Quantitative dissection of hydrogen bond-mediated proton transfer in the ketosteroid isomerase active site. *Proc. Natl. Acad. Sci.*, 2013, **110**, E2552–E2561.

126. Bhatt, H., Mishra, A. K., Chitra Murli, Verma, A. K., Garg, N., Deo, M. N. and Sharma, S. M., Proton transfer aiding phase transitions in oxalic acid dihydrate under pressure. *Phys. Chem. Chem. Phys.*, 2016, **18**, 8065–8074.

127. Bhatt, H. *et al.*, Hydrogen bond symmetrization in glycinium oxalate under pressure. *J. Phys. Chem. B*, 2016, **120**, 851−859.

128. Takahashi, T. and Bassett, W. A., Bassett high-pressure polymorph of iron. *Science*, 1964, **145**, 483–489.

129. Hemley, R. J., Bell, P. M. and Mao, H. K., Laser techniques in high-pressure geophysics. *Science*, 1987, **237**, 605–612.

130. Hemley, R. J., Ho-kwang Mao, Shen, G., Badro, J., Gillet, P., Hanfland, M. and Häusermann, D., X-ray imaging of stress and strain of diamond, iron, and tungsten at megabar pressures. *Science*, 1997, **276**, 1242–1245.